Coordination of Ethylamine on Small Silver Clusters: Structural and Topological (ELF, QTAIM) Analyses

Corinne Lacaze-Dufaure, Yann Bulteau, Nathalie Tarrat, David Loffreda, Pierre Fau, Katia Fajerwerg, Myrtil L Kahn, Franck Rabilloud, Christine Lepetit

Coordination of ethylamine on small silver clusters: structural and topological (ELF, QTAIM) analyses

Corinne Lacaze-Dufaure[a]*, Yann Bulteau[a], Nathalie Tarrat[b]*, David Loffreda[c], Pierre Fau[d], Katia Fajerwerg[d], Myrtil L. Kahn[d], Franck Rabilloud[e], Christine Lepetit[d]*

a : CIRIMAT, Université de Toulouse, CNRS, INP- ENSIACET 4 allée Emile Monso - BP44362, 31030 Toulouse cedex - France.

b : CEMES, Université de Toulouse, CNRS, 29 rue Jeanne Marvig, Toulouse 31055, France

c : Univ Lyon, Ens de Lyon, CNRS UMR 5182, Université Claude Bernard Lyon 1, Laboratoire de Chimie, F-69342 Lyon, France

d : LCC-CNRS, Université de Toulouse, CNRS, UPS, Toulouse, France.

e : Univ. Lyon, Université Claude Bernard Lyon 1, CNRS, Institut Lumière Matière, F-69622, Villeurbanne, France

corinne.dufaure@ensiacet.fr

nathalie.tarrat@cemes.fr

christine.lepetit@lcc-toulouse.fr

Keywords: Ag clusters, geometrical 2D/3D transition, Ethylamine, DFT, Ag-N and Ag-Ag bond energies, ELF and QTAIM topological analyses.

Abstract

Amine ligands are expected to drive the organization of the metallic centers as well as the chemical reactivity of the silver clusters early growing during the very first steps of the synthesis of silver nanoparticles via an organometallic route. DFT (Density Functional Theory) computational studies have been performed in order to characterize the structure, the atomic charge distribution and the planar (2D)/three-dimensional (3D) relative stability of small-size silver clusters (Ag_n, $2 \leq n \leq 7$), with or without an ethylamine (EA) ligand coordinated to the Ag clusters. The transition from 2D to 3D structures is shifted from n = 7 to n = 6 in the presence of one EA coordinating ligand and it is explained from the analysis of the Ag-N and Ag-Ag bond energies. For fully EA saturated silver clusters ($Ag_n - EA_n$) the effect on the 2D/3D transition is even more pronounced with a shift between n = 4 and n = 5. Subsequent ELF (Electron Localization Function) and QTAIM (Quantum Theory Atoms in Molecules) topological analyses allow for the fine characterization of the dative Ag-N and metallic Ag-Ag bonds, both in nature and strength. Electron transfer from the ethylamine to the coordinated silver atoms induces an increase of the polarization of the metallic core.

INTRODUCTION

Silver nanoparticles (AgNPs) are increasingly used and their optical, electrochemical and biomedical applications are strongly related to their size and shape.[1,2] AgNPs may be prepared using a physical or chemical routes. Among the latter, synthesis of colloidal nanoparticles can involve a precursor complex which is reduced in the presence of stabilizing ligands. Such ligands prevent the nanoparticles' coalescence in solution by the formation of a shell of organic dispersant around them. [3,4]

Recent studies of AgNPs obtained from the hydrogenolysis , at moderate temperature (T< 373K), of silver-amidinate complexes have evidenced the stabilizing synergy between the amidine released from the precursor complex, and the long alkyl chain amine ligands such as hexadecylamine (HDA).[5] The strong affinity of the amidine molecule for the AgNPs surface has been evidenced by the combination of Surface Enhanced Raman Spectroscopy (SERS), nuclear magnetic resonance (NMR) measurements and simulations of Ag-amines Raman spectra.**[5]** In contrast, short-time-scale fluxional interactions between the AgNPs surface and the HDA molecules have been highlighted.**[5]** However, the amine ligands play a predominant role for the stabilization of stable colloidal Ag solutions, and they are therefore involved in the very first steps of the Ag nanocrystals formation.

The study of the early growing species, resulting from the nucleation and growth of the very first nuclei, can help to understand and control the very first steps of the AgNPs synthesis. To date, a detailed understanding at the atomic scale of such processes is clearly missing in the literature. Silver clusters are therefore attractive targets for investigating the role played by amines at the very beginning or at the end of the synthesis of AgNPs. In that context, the influence of an amine ligand on the structure and stability of Ag very first nuclei will be investigated in this work, by studying the interaction of a model amine (ethylamine EA), with small planar (2D) or three-dimensional (3D) Ag_n clusters ($2 \leq n \leq 7$).

A key and challenging point of this work is to go as far as unraveling the nature of the bonds involved in these aggregates. Indeed, although clusters up to several hundreds of silver atoms have been extensively studied in vacuum at various calculation levels, including semi-empirical methods,[6] density functional tight binding (DFTB),[7,8] density functional theory (DFT)[9] or time-dependent DFT for optical properties[10] or *ab initio* methods such as coupled cluster (CCSD) theory,[11] only few of these theoretical studies were devoted to the study of chemical bonding inside the AgNPs or between the AgNPs and their outer-shell protecting ligands. **[2-4,]**[12-14]

To fill this gap, various theoretical approaches and topological analyses can be considered for the chemical bonding analysis of these systems such as: the Molecular Orbital (MO) analysis,[15] the Energy Decomposition Analysis (EDA),[16] the Valence Bond (VB) method,[17] Electron Localization Function (ELF)[18,19] and Quantum Theory of Atoms In Molecules (QTAIM)[20]. Topological analyses will be preferred in this work, because the chemical bonding assignment on the basis of ELF and QTAIM descriptors is more straightforward.[21] ELF and QTAIM descriptors, allowing to discriminate between ionic, weakly covalent,[22] and dative (also known as coordinate bond) Ag-N bonds and describing finely the metallic Ag-Ag bonds, have already been successfully used to characterize the bonding and bond strength in some silver precursor complexes and in small silver clusters.[23]

The paper is organized as follows. After a brief description of the computational methods used, the structure and the relative stability of 2D or 3D Ag_n clusters are studied together with the charge distribution and reorganization, in the absence and presence of one amine ligand. Moreover, the effect of EA saturation ($Ag_n - EA_n$) on the transition between 2D and 3D geometry of the silver cores is investigated. Finally, ELF and QTAIM topological descriptors of Ag-N and Ag-Ag bonds are discussed in a third section.

COMPUTATIONAL DETAILS

DFT calculations

Spin-polarized DFT calculations were performed using the Vienna *ab initio* simulation package (VASP[24-26]) with periodic boundary conditions and pseudopotentials based on the projector augmented wave method (PAW[27,28]). Note that this work is the starting point of a multiscale study aiming at investigating the evolution of the interaction between a silver nanoparticle and an amine ligand over a size range corresponding to a few silver atoms up to several hundreds. As localized bases do not allow the study of metal nanoparticles containing more than a few dozen atoms, all the calculations were performed using a plane wave basis set.

As advised in the bibliography concerning the adsorption of small molecules on Ag_n clusters,[29-31] a dispersion-corrected functional was used, *i.e.* the optB86b-vdw functional.[32] In this functional, the dispersion interaction is directly obtained from the electron density by adding a non-local term to the local correlation functional. The simulation box sizes have been chosen in order to avoid any interaction between the simulated models and their periodic images (25 x 25 x 30 Å^3 for Ag_n and $Ag_n - EA$ and 35 x 35 x 40 Å^3 for $Ag_n - EA_n$) . A plane wave kinetic energy cutoff of 600 eV was used and the atomic positions were relaxed until the forces

reached a value lower than 5.10^{-3} eV $Å^{-1}$. Due to the molecular nature of the explored clusters, total electronic energies of these systems have been calculated at the gamma point of the Brillouin zone. For dealing with the partial occupancies around the Fermi level, a Methfessel-Paxton smearing was used (with sigma = 0.01 eV).[33]

From the total energies E of the naked Ag_n clusters or of the related $Ag_n - EA$ and $Ag_n - EA_n$ systems, the energy differences $\Delta E_{2D/3D}$ in absence or in presence of EA were determined as:

$$\Delta E_{2D/3D}^{Agn} = E(Ag_n^{2D}) - E(Ag_n^{3D})$$

$$\Delta E_{2D/3D}^{Agn-EA} = E(Ag_n^{2D} - EA) - E(Ag_n^{3D} - EA)$$

$$\Delta E_{2D/3D}^{Agn-EAn} = E(Ag_n^{2D} - EA_n) - E(Ag_n^{3D} - EA_n)$$

The cohesive energy per Ag atom $E_{coh/atom}^{Agn}$ of the Ag_n^{2D} and Ag_n^{3D} clusters was calculated for the naked clusters:

$$E_{Coh/atom}^{Agn} = (E(Ag_n) - nE(Ag))/n$$

where $E(Ag_n)$ is the energy of the bare relaxed Ag_n cluster (2D or 3D geometry), $E(Ag)$ is the energy of an Ag atom in vacuum and *n* the number of Ag atoms in the cluster.

Similarly, the cohesive energy per bond $E_{Coh/bond}^{Agn}$ is defined by:

$$E_{Coh/bond}^{Agn} = (E(Ag_n) - nE(Ag))/N$$

where *N* is the number of Ag-Ag bonds in the cluster corresponding to an Ag-Ag distance lower than two times the Ag covalent radius, *i.e.* 3.4 Å.[34]

The coordination energies E_{coord} and the binding energies E_{bind}, defined hereafter, are expected to characterize the strength of the interaction between EA and the Ag_n cluster:

$$E_{coord} = E(Ag_n - EA) - E(Ag_n) - E(EA)$$

where $E(Ag_n - EA)$ is the total energy of the $Ag_n - EA$ system and $E(EA)$ is the energy of the EA molecule optimized in vacuum. The binding energy characterizes the strength of the binding between EA and the silver cluster without taking into account the deformation of both fragments occurring upon coordination:

$$E_{bind} = E(Ag_n - EA) - E_{SP}(Ag_n) - E_{SP}(EA)$$

where $E_{SP}(Ag_n)$ and $E_{SP}(EA)$ are respectively the single point (SP) energies of isolated Ag_n and of EA in their coordinated geometry.

Topological analyses

Topological methods are based on the analysis of the gradient field of a local function within the dynamic field theory and provide a partition of the molecular space into non-overlapping basins.

The topological analysis of the electron density $\rho(r)$, designed as the Quantum Theory of Atoms in Molecules (QTAIM) by R. Bader, yields atomic basins and QTAIM atomic charges.[20]

First, the QTAIM atomic charges resulting from the Bader's population analysis on VASP charge densities[35-38] was used to quantify the electronic changes upon EA coordination to the silver clusters by:

(i) the atomic charge variation for one atom X of the EA molecule $\Delta q_X = q_X(Ag_n - EA) - q_X(EA)$,

(ii) the total charge variation of the EA ligand, namely, $\Delta Q_{EA} = Q_{EA}^{coord} - Q_{EA}^{free}$

In a second time, the electronic structure of geometries optimized with VASP were calculated at the PBE-D3/def2TZVP level of calculation using Gaussian09.[39] This level of calculation was indeed shown to yield geometries in good agreement with the periodic DFT calculations on few calibration studies (Figure S1, See Supporting Information).

The QTAIM topological analysis allows defining bond paths and bond critical points (BCPs). The nature of the chemical bond is characterized from various properties of the electron density at the BCPs, especially the sign of the Laplacian of the electron density and the values of the kinetic energy density ($\boldsymbol{G_{bcp}}$), of the potential energy density ($\boldsymbol{V_{bcp}}$) and of the energy density $\boldsymbol{H_{bcp} = G_{bcp} + V_{bcp}}$, following the Bianchi's[40] and Macchi's classification.[41] Negative and positive values for the Laplacian of the electron density at the BCP are assigned to « electron-shared » and « closed-shell » interactions, respectively.[20] Bianchi *et al.*[40] distinguish three bonding regimes, depending on the value of the absolute ratio of the potential energy density to the kinetic energy density ($|\boldsymbol{V}_{\mathbf{bcp}}|/\boldsymbol{G}_{\mathbf{bcp}}$). The intermediate bond regime ($1 < |\boldsymbol{V}_{\mathbf{bcp}}|/\boldsymbol{G}_{\mathbf{bcp}} < 2$) lies between electron-shared covalent bonds ($|\boldsymbol{V}_{\mathbf{bcp}}|/\boldsymbol{G}_{\mathbf{bcp}}$ greater than 2) and closed-shell ionic bonds or van der Waals interactions ($|\boldsymbol{V}_{\mathbf{bcp}}|/\boldsymbol{G}_{\mathbf{bcp}}$ lower than 1) and includes dative bonds and ionic bonds of weak covalent character. The Macchi's classification relies on the values of both local descriptors and the delocalization index (DI) and offers a way to refine the bond characterization further. The covalence degree may be estimated from the latter and from ($|\boldsymbol{H}_{bcp}|/\boldsymbol{\rho}_{bcp}$).[40b] The strength of the interaction may be estimated from the correlation scheme of Espinosa *et al.* [42] providing the corresponding positive interaction energy (E_{int}= - ½ $\mathbf{V_{bcp}}$, with E_{int} (eV) = -13.606 x $\mathbf{V_{bcp}}$ (au)). Interacting Quantum Atoms (IQA)

analysis[43] was performed to get insight into the relative contributions of electron sharing and electrostatic interactions of the metallic Ag-Ag bonds. Within the IQA energy decomposition scheme, using QTAIM atoms, the total energy of the system is decomposed into intra-atomic and interatomic contributions.[44] The interatomic interactions energy, E^{IQA}_{int} (A, B) (A ≠ B), is further partitioned as E^{IQA}_{int} (A, B) = V^{IQA}_{cl} (A, B) + V^{IQA}_{xc} (A, B). V^{IQA}_{cl} (A, B), called the classical term, is related to the electrostatic component of the A-B interaction, while V^{IQA}_{xc} (A, B), known as the exchange-correlation term, refers to electron sharing due to quantum mechanics effects that also incorporate Pauli Exclusion Principle and may be related to the covalence degree of the bond. IQA analyses have been shown to be useful for characterizing non-covalent interactions.[45] QTAIM and IQA analyses were performed with the AIMAll software.[46]

The electron localization function (ELF) measures the excess of kinetic energy because of the Pauli repulsion.**[18]** ELF values are confined between 0 and 1. ELF is close to 1 in regions where electrons are single or form antiparallel spin pairs, whereas it tends to 0 in regions where the probability to find parallel spin electrons close to one another is high.**[19]** ELF tends to 1 in those regions where the electron localization is high (atomic shells, chemical bonds and lone electron pairs),[47] whereas it tends to small values at the boundaries between these regions.[48] The topological analysis of the ELF gradient field yields a partition of the molecular space into non-overlapping electronic domains, basins of attractors, classified into core, valence bonding and nonbonding basins. The attractors, namely local maxima of the ELF function, can be single points (general case), circles or spheres depending on the symmetry.**[19]** These basins are in one-to-one correspondence to the core, lone or shared pairs of the Lewis model. A core basin contains a nucleus X (except a proton) and is designated as C(X). A valence bonding basin lies between two or more core basins. Valence basins are further distinguished by their synaptic order, which is the number of core basins with which they share a common boundary. The monosynaptic basins denoted as V(X), correspond to lone pairs, whereas the di- and polysynaptic ones are related to bi- or multi-centric bonds, denoted as V(X1, X2, X3. ...). The average population of the basin is obtained by integration of the one-electron density over the basin volume. A statistical population analysis allows for considering the variance and the covariance of the basin populations, which are related to the electron delocalization.[49] The populations do not take integral values and are about twice the topologically-defined Lewis bond orders for bonding valence basins.**[49,50]** The populations and (co)variances of these valence basins can be further interpreted in terms of weighted combinations of mesomeric structures. **[19, 49,50]** ELF topological analysis was performed with the TopMoD package.[51]

RESULTS AND DISCUSSION

1. Structures and relative stability of 2D or 3D Ag_n clusters ($2 \leq n \leq 7$)

The influence of the ethylamine coordination on the geometry and on the 2D/3D geometrical transition of the Ag_n clusters ($2 \leq n \leq 7$) was first studied on the basis of energy analyses.

The most stable geometries calculated for planar Ag_n^{2D} and three-dimensional Ag_n^{3D} clusters, shown in Figure 1, are in good agreement with previous reports.[11,52-59]

For Ag_3, if we compare the total energies of the different isomers, the equilateral geometry is found to be less stable than the most stable isosceles triangle by 0.914 eV. It is indeed known that the equilateral geometry is a conical intersection which leads to Jahn-Teller distorsions.[11] The isosceles triangle with one angle of 68.6°, and two angles of 55.7° is the most stable form, in agreement with Fournier's reports[55] (VWN calculations), and Gamboa *et al.*'s works (PBE computations) [54], whereas McKee *et al.*[59] described the most stable trimer geometry as an isosceles triangle with a vertex angle of 54.9° (M06 calculations). Chen *et al.*[11] found as the most stable trimers an isosceles triangle with a vertex angle of 75.7° in the framework of B3LYP calculations and an isosceles triangle with a vertex angle of 67.7° thanks to CCSD(T). No stable 3D geometry could be determined for the tetramer Ag_4, whereas 2D and 3D stable forms could be determined for Ag_5, Ag_6 and Ag_7 clusters. A hexagonal planar geometry of Ag_7^{2D} could not be localised on the potential energy surface.

The Ag-Ag distances (2.561-2.958 Å range with 97% of the Ag-Ag distances between 2.623 and 2.788 Å), are consistent with previous computational studies (2.56-3.03 Å for PBE calculations)[54]. These values can differ significantly from Ag-Ag distances in the FCC Ag bulk (2.889 Å[60]). The nature of the corresponding Ag-Ag bonds will be analysed later.

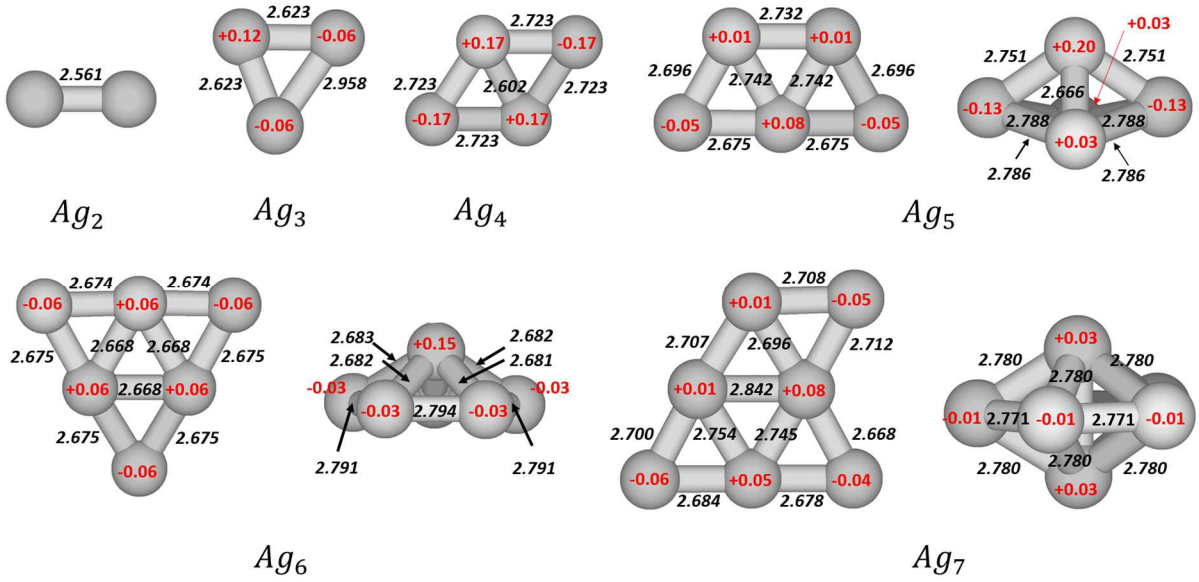

Figure 1. Most stable geometries of Ag_n^{2D} and Ag_n^{3D} clusters calculated in the present work. Bond lengths in Å (*in black*) and QTAIM atomic charges in *e* (in red)

The energy differences $\Delta E_{2D/3D}^{Agn}$ between Ag_n^{2D} and Ag_n^{3D} clusters are presented in Table 1. The 2D/3D geometrical transition is observed between n = 6 and n = 7. For Ag_5 and Ag_6, the 2D structure is respectively 0.472 eV and 0.172 eV more stable than the 3D geometry, consistently with previous works. For instance, Fournier[55] found $\Delta E_{2D/3D}^{Agn}$values of about -0.52 eV and -0.23 eV for Ag_5 and Ag_6 respectively (standard LSD framework) and McKee *et al.*[59] determined a $\Delta E_{2D/3D}^{Agn}$value of about -0.16 eV for Ag_6 (M06 computations). Singh *et al.*[57] calculated values of -0.65 eV and -0.26 eV (vdW-DF2 calculations) for Ag_5 and Ag_6 respectively. Chen *et al.*[11] calculated an enhanced stability of 0.43 eV and 0.19 eV respectively for Ag_5^{2D} and Ag_6^{2D} clusters over 3D ones thanks to CCSD(T) calculations. In the present work, we also observe a decrease of the stability of the 2D form over the 3D form when *n* increases and the Ag_7^{3D} cluster is more stable of 0.669 eV than the 2D one. This value compares well with the work of McKee *et al.* [59] ($\Delta E_{2D/3D}^{Ag7}$= 0.61 eV, M06 calculations), Chen *et al.*[11] ($\Delta E_{2D/3D}^{Ag7}$= 0.72 eV) but is notably higher than the value of Singh *et al.* [57] ($\Delta E_{2D/3D}^{Ag7}$ = 0.11 eV, vdW-DF2 calculations).

Table 1. Selected energy data (in eV) of Ag_n and Ag_n-EA clusters ($2 \leq n \leq 7$). Variation of the total charge of EA ΔQ_{EA} (in e) estimated from the QTAIM atomic charges. Ag-N distances (in Å). OptB86b-vdW level of calculation.

Compounds	$E_{2D/3D}^{Agn}$	$\Delta E_{2D/3D}^{Agn-EA}$	E_{coord}	E_{bind}	ΔQ_{EA}	Ag-N distance
$Ag - EA$			-0.401	-0.409	+0.10	2.419
$Ag_2 - EA$			-0.773	-0.782	+0.14	2.283
$Ag_3 - EA$			-0.973	-1.005	+0.15	2.253
$Ag_4^{2D} / Ag_4^{2D} - EA$			-1.015	-1.033	+0.15	2.248
$Ag_5^{2D} / Ag_5^{2D} - EA$	-0.472	-0.027	-0.699	-0.715	+0.14	2.302
$Ag_5^{3D} / Ag_5^{3D} - EA$			-1.144	-1.170	+0.17	2.234
$Ag_6^{2D} / Ag_6^{2D} - EA$	-0.172	0.024	-0.682	-0.699	+0.13	2.319
$Ag_6^{3D} / Ag_6^{3D} - EA$			-0.878	-0.928	+0.14	2.292
$Ag_7^{2D} / Ag_7^{2D} - EA$	0.669	0.593	-0.765	-0.782	+0.14	2.303
$Ag_7^{3D} / Ag_7^{3D} - EA$			-0.689	-0.714	+0.13	2.325

The cohesive energy per Ag atom $E_{Coh/atom}^{Agn}$ of Ag_n^{2D} and Ag_n^{3D} *versus* the number of silver atoms *n* ($2 \leq n \leq 7$) is presented in Figure 2. It decreases with increasing number of atoms *n*, suggesting a stronger binding (and so a greater stability) when the Ag_n cluster is growing. A 3D growth becomes more favourable than the 2D one for *n* equal to 7.

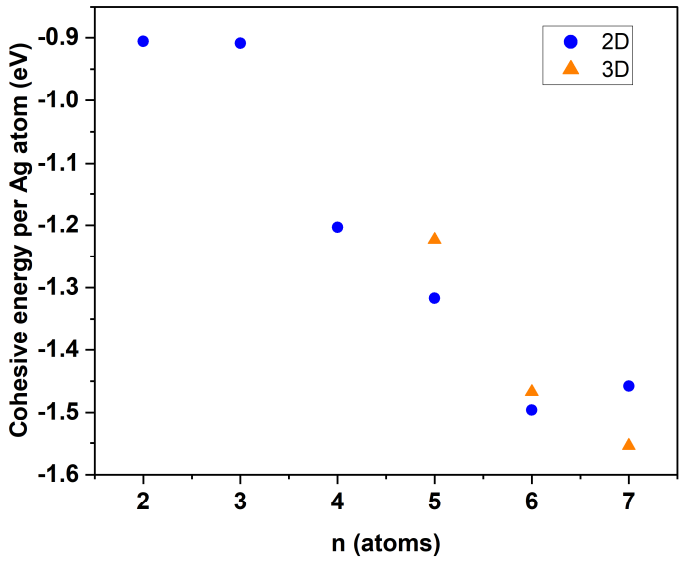

Figure 2. Cohesive energies per atom $E_{Coh/atom}^{Agn}$ (in eV) of the Ag_n clusters. OptB86b-vdW level of calculation.

The variation of the cohesive energy per Ag-Ag bond as a function of the number of Ag atoms in the Ag_n cluster is displayed in Figure 3. For n > 4, the Ag-Ag bonding is stronger in Ag_n^{2D} ($E_{Coh/bond}^{Agn}$ = -0.962 ± 0.035 eV) than in Ag_n^{3D} ($E_{Coh/bond}^{Agn}$ = -0.780 ± 0.100 eV). For Ag_5^{2D}/Ag_5^{3D} (resp. Ag_6^{2D}/Ag_6^{3D}) the number of bonds in the cluster is 7/8 (resp. 9/10). The small increase of the number of bonds in the 3D cluster does not compensate the weaker strength of the Ag-Ag bonds. In the case of the Ag_7 cluster, the number of Ag-Ag bonds increases from 11 in Ag_7^{2D} to 16 in Ag_7^{3D}, and the 3D cluster becomes the most stable one even if the Ag-Ag bonds are weaker when compared to the 2D isomer.

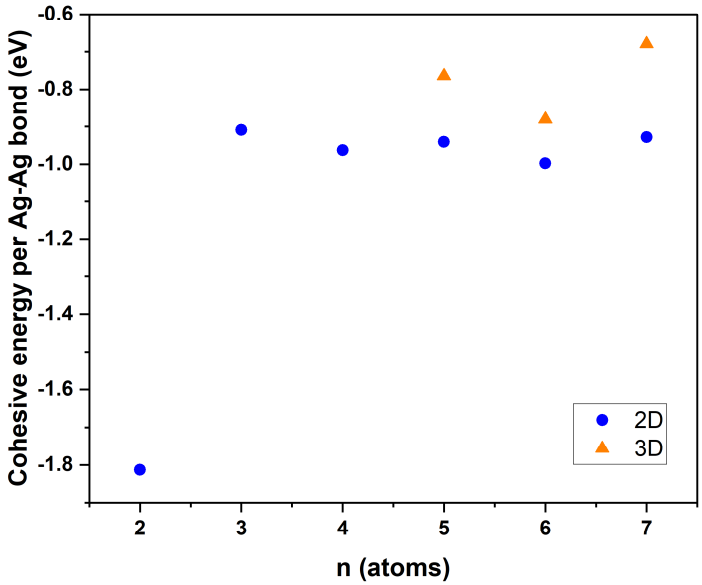

Figure 3. Cohesive energies per Ag-Ag bond $E_{Coh/bond}^{Agn}$ (in eV) of the Ag_n clusters. OptB86b-vdW level of calculation.

The QTAIM atomic charges of each Ag atom of the Ag_n cluster are displayed in Figure 1. The latter are slightly polarized with small positive charges on Ag atoms of the cluster with the larger coordination number (0.12 e in Ag_3, 0.17 e in Ag_4, 0.08 and 0.10 e in Ag_5^{2D} and 0.20 e in Ag_5^{3D}, 0.06 e in Ag_6^{2D} and 0.15 e in Ag_6^{3D}, 0.08 e in Ag_7^{2D} and 0.03 e in Ag_7^{3D}) and negative charges on the Ag atoms with the smaller coordination number. It is worth noting that in Ag_7^{3D}, the coordination number of all the Ag atoms is equal or larger than 4, and it leads to a very weak electronic transfer between the Ag atoms, lower than 0.03 *e*.

2. Structures and relative stability of $Ag_n - EA_m$ clusters ($2 \leq n \leq 7$, m = 1 or n)

The influence of the coordination of a single ethylamine ligand on the geometry and 2D/3D geometrical transition of the Ag_n clusters ($2 \leq n \leq 7$) is discussed hereafter.

The calculated structure of ethylamine (most stable conformer) in vacuum is shown in Figure 4. The N1-C2 and C2-C3 bond lengths are 1.467 and 1.531 Å respectively. The net charge on the N atom is -1.08 *e* and the net charge on the C atoms are +0.36 *e* (C2) and -0.14 *e* (C3). The H atoms bound to the C2 and C3 atoms exhibit a slightly cationic character (QTAIM charge of

+0.04 *e* and +0.02 *e* respectively) while the QTAIM charge of H atoms bound to the N atoms is significant (+0.36 *e*).

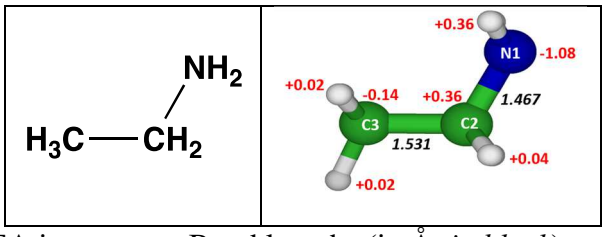

Figure 4. Structure of EA in vacuum. Bond lengths (in Å, *in black*) and QTAIM charges (in *e,* in red). OptB86b-vdW level of calculation. Carbon atoms in green, nitrogen atom in blue and hydrogen atoms in white.

The coordination energies E_{coord}, and binding energies E_{bind} in $Ag_n - EA$ systems are given in Table 1 and their most stable calculated structures are shown in Figure 5. For $Ag_n - EA$ aggregates with n ≥ 2, starting from structures with the EA coordinated in a bridging mode to two silver atoms or in a threefold mode, the calculation always converged towards the same on-top geometries presented in Figure 5. This is consistent with previous theoretical studies[13] and photodissociation experiments,[61] showing that NH_3 is bound end-on to silver clusters. The average calculated Ag-N distance is 2.284 ± 0.041 Å. The Ag-N distance decreases from 2.419 Å in $Ag - EA$ to 2.234 Å in $Ag_5^{3D} - EA$ while the $Ag_n - EA$ bond strength increases (E_{coord} varies from -0.401 eV to -1.144 eV, see in Table 1). For the less stable $Ag_5^{2D} - EA$, $Ag_6^{2D} - EA$ and $Ag_7^{2D} - EA$, and for the most stable $Ag_6^{3D} - EA$, and $Ag_7^{3D} - EA$ systems, the average Ag-N distance is 2.308 ± 0.017 Å and the $Ag_n - EA$ interaction remains quasi-constant (coordination energy in the range -0.682 to -0.878 eV). These Ag-N bond lengths are in the range of previous reports on related systems, namely, 2.1 to 2.4 Å[13,62-64]. In the $Ag_n - EA$ systems, there is free rotation around the N-C bond (rotation barrier lower than 60 meV for all the clusters). There is no interaction between the ethyl moiety and the silver atoms. The shortest NH---Ag distance in $Ag_n - EA$ systems is of 2.856 Å (in $Ag - EA$) and it is larger than the sum of van der Waals radii of H and Ag (1.1 + 1.7 = 2.8 Å)[34] ruling out any agostic-type Ag-H bond (the distance H-Ag for the bonding on an H atom on Ag(111) is shorter than 1.925 Å[65] and the Ag-H bond length in the silver hydride is 1.618 Å[66]).

In the $Ag_n - EA$ systems of Figure 5, the N1-C2 distance of 1.484 ± 0.005 Å is slightly longer of about 0.02 Å than in the free EA (1.467 Å, see Figure 4), while the C2-C3 distance of 1.531 Å (Figure 4), remains almost unchanged upon bonding to Ag (maximum variation of about 0.007 Å).

The Ag-Ag bonds adjacent to the silver atom coordinated to EA are slightly lengthened (by less than 0.05 Å) as compared to the corresponding ones in the bare cluster, and the other Ag-Ag bonds are little shortened conversely (by less than 0.06 Å) except for $Ag_3 - EA$ exhibiting a variation of 0.17 Å.

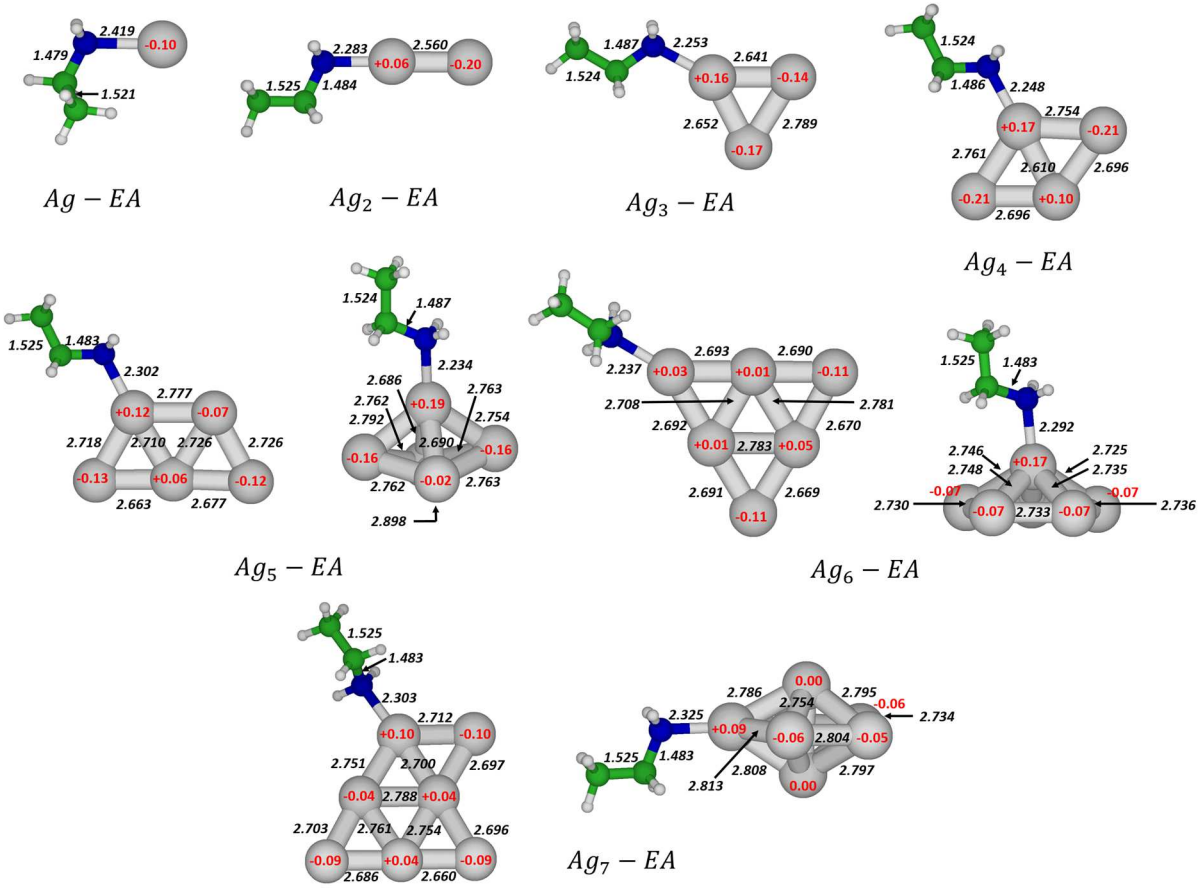

Figure 5. Most stable geometries of $Ag_n^{2D} - EA$ and $Ag_n^{3D} - EA$ calculated in the present work. Bond lengths (in Å, *in black*) and QTAIM atomic charges (in *e,* in red). OptB86b-vdW level of calculation.

The relative energies $\Delta E_{2D/3D}^{Agn-EA}$ are given in Table 1. Similar to the parent Ag_7 clusters, the 3D structure of $Ag_7^{3D} - EA$, is more stable by 0.593 eV than the one of $Ag_7^{2D} - EA$. In contrast, 2D and 3D structures are quasi-degenerate in energy for $Ag_5 - EA$ and $Ag_6 - EA$ clusters (2D/3D relative energies are calculated to be – 0.027 and +0.024 eV respectively). The geometrical 2D-3D transition observed between n = 6 and n = 7 for the Ag_n clusters, is therefore shifted between n = 5 and n = 6 upon EA- coordination.

The coordination energy E_{coord} characterises the overall process of the adsorption of EA on the Ag_n clusters, including the deformation of the EA molecule and of the clusters. The latter can be quantified by the deformation energies, E_{def}^{EA} and $E_{def}^{cluster}$ respectively, and the interaction between both fragments by the binding energy E_{bind}. The deformation energies values are presented in Table S2. The geometries of EA and Ag_n clusters ($2 \leq n \leq 7$) are little modified in the bonding process, as shown in Figure 5 and by their weak deformation energies, namely 6 - 41 meV range for Ag_n ($2 \leq n \leq 7$) and 8 - 13 meV range for EA (Table S2). The coordination energy E_{coord} of the EA ligand on Ag_n clusters comes thus mainly from the interaction between both fragments and is weakly influenced by their deformation. The values of E_{coord} for the Ag_n^{2D} clusters decrease from n = 1 to 4 (with coordination energies that vary from -0.401 eV to -1.015 eV) and is about -0.732 ±0.033 eV for n = 5 to 7. For the Ag_n^{3D} clusters, the coordination energy increases from n = 5 (-1.144 eV) to n = 7 (-0.689 eV) showing a lowering of the interaction between the EA molecule and Ag_n clusters. The calculated values of the coordination energy are in agreement with the ones reported for the bonding of ammonia on small-size Ag_n clusters. Martinez *et al.* reported coordination energies ranging from -0.36 to -0.94 eV[13] for the bonding of NH_3 on Ag_n (n = 1 - 4). Bond energies ranging from -0.70 to -0.31 eV for the bonding of NH_3 on Ag_2 to Ag_7 were reported by Rayer *et al.* from experimental measurements.[61]

The variation of E_{bind} in Figure 6 is similar to the variation of E_{coord} given in Table 1. The binding energy between Ag_n and EA is stronger for the 3D clusters with n = 5 (0.455 eV) and n = 6 (0.229 eV), while it is stronger for the 2D clusters with n = 7 (0.068 eV). However, the 2D/3D relative energies are suggesting isoenergetic $Ag_5^{2D} - EA$ and $Ag_5^{3D} - EA$ systems, and isoenergetic $Ag_6^{2D} - EA$ and $Ag_6^{3D} - EA$ systems because of the compensation between the coordination energies ($\Delta E_{coord}^{2D/3D}$ = 0.445 eV and 0.196 eV respectively) and the relative stability of 2D and 3D structures ($\Delta E_{2D/3D}^{Agn}$ values of -0.472 eV and -0.172 eV respectively).

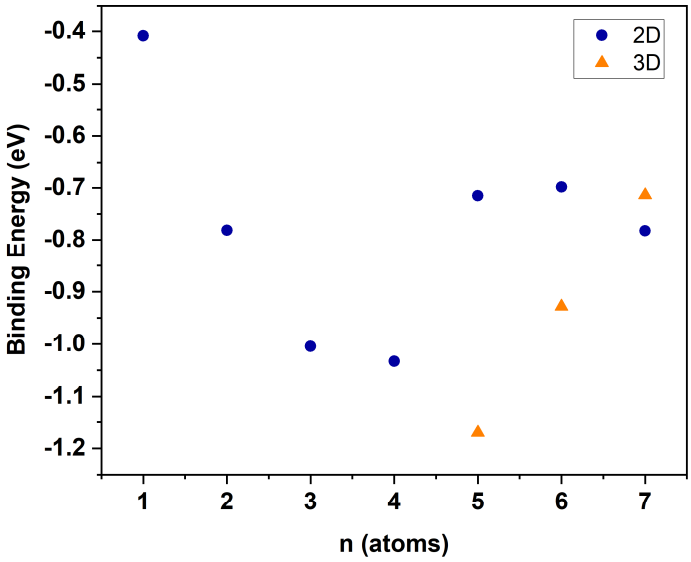

Figure 6. Binding energies E_{bind} (in eV) of $Ag_n - EA$ clusters ($2 \leq n \leq 7$). OptB86b-vdW level of calculation.

During the bonding process, the total charge variation of the EA ligand is about 0.14 ± 0.04 *e*, showing that there is a weak electron transfer from the EA ligand to the Ag_n core of the $Ag_n^{2D} - EA$ and $Ag_n^{3D} - EA$ clusters. This is consistent with the slight variation of the EA and Ag_n geometries and the small values of deformation energies. The variation of the atomic charges of N1 (lower than 0.05 *e*), C2 (lower than -0.09 *e*) and C3 (lower than 0.12 *e*) atoms of the EA (presented in Table 2), are indicative of very weak electron density reorganisations in the molecule.

Table 2. QTAIM atomic charges q_X and charges variation Δq_X (in *e)* of N and C atoms in the EA molecule during the coordination of EA on Ag_n clusters ($2 \leq n \leq 7$). OptB86b-vdW level of calculation.

$Ag_n/Ag_n - EA$	q_{N1}	Δq_{N1}	q_{C2}	Δq_{C2}	q_{C3}	Δq_{C3}
$Ag - EA$	-1.05	+0.03	+0.32	–0.04	-0.05	+0.09
$Ag_2 - EA$	-1.04	+0.04	+0.31	–0.05	-0.03	+0.11
$Ag_3 - EA$	-1.04	+0.04	+0.30	–0.06	-0.11	+0.03
$Ag_4^{2D} / Ag_4^{2D} - EA$	-1.03	+0.05	+0.31	–0.05	-0.11	+0.03
$Ag_5^{2D} / Ag_5^{2D} - EA$	-1.03	+0.05	+0.27	–0.09	-0.05	+0.09
$Ag_5^{3D} / Ag_5^{3D} - EA$	-1.05	+0.03	+0.29	–0.07	-0.05	+0.09
$Ag_6^{2D} / Ag_6^{2D} - EA$	-1.06	+0.02	+0.34	–0.02	-0.12	+0.02
$Ag_6^{3D} / Ag_6^{3D} - EA$	-1.06	+0.02	+0.29	–0.07	-0.08	+0.06
$Ag_7^{2D} / Ag_7^{2D} - EA$	-1.07	+0.01	+0.29	–0.07	-0.02	+0.12
$Ag_7^{3D} / Ag_7^{3D} - EA$	-1.07	+0.01	+0.30	–0.06	-0.05	+0.09

The above geometry and energy data show that the EA ligand modifies the properties of Ag_n clusters. The electronic transfer from EA towards the Ag_n core is a first indication of the formation of an iono-covalent Ag-EA bond and of the chemisorption of the EA ligand on the Ag_n^{2D} or Ag_n^{3D} clusters.

To get closer to the experimental conditions, in which the silver nuclei are surrounded by a large number of amine ligands, we investigated the effect of EA saturation of the Ag_n clusters on their 2D/3D transition. $Ag_n - EA_n$ systems with n = 4 to 6 were studied and the results suggest an earlier 2D/3D transition than in the case of the bare clusters or of the mono-coordinated $Ag_n - EA$ ones. The most stable 2D and 3D geometries are presented in Figure S2. As the effect of the ligand saturation on the silver cores is strong, the optimisation protocol was adapted for the determination of 2D structures as a direct optimisation led to distorted silver cores. A two-steps approach was used, i.e. a first partial optimisation of the amines ligands (with frozen 2D Ag core) followed by an unconstrained optimisation of the whole $Ag_n - EA_n$ systems.

In $Ag_4 - EA_4$, the 2D rhombic geometry is the stable one and the 3D tetrahedral structure could not be localised, whereas the 3D structures are more stable than the 2D ones for the silver cores of $Ag_5 - EA_5$ (distorted pyramid more stable than 2D structure by 0.088 eV) and of $Ag_6 - EA_6$ (distorted pentagonal pyramid more stable than 2D triangle by 0.250 eV). In the experimental conditions, the formation of a 3D nucleus could thus occur from 5 Ag atoms, i.e. at the very beginning of the NPs synthesis

3. ELF and QTAIM topological analyses

In this section, the bonding of the ethylamine by interaction of the amino group -NH_2 to a vertex of the Ag_n cluster, is more finely characterized by QTAIM and ELF topological analyses. Calibrations studies were first performed in order to select the calculation level for the present molecular approach to be consistent with the above periodic DFT approach. The results are given in the Figure S1 (See Supporting Information). The PBE-D3/def2TZVP level of calculation yielded the best agreement between optimized geometries (Figure S1) and was used to re-calculate the electronic structures of geometries optimized with VASP ($Ag - EA$, Ag_2, $Ag_2 - EA$) and to calculate the geometry of $Ag_2 - EA_2$. The latter complex was added to the above series in order to get closer to the experimental conditions (i.e., NPs encapsulated in an amine shell) by considering a saturated silver dimer.

Table 3. QTAIM descriptors (in a.u.) of the bond critical points (bcp) related to Ag-N bonds in $Ag-EA$, Ag_2-EA, Ag_2-EA_2 compounds. BCP location is illustrated for Ag_2-EA in Figure 7. [a]: Potential energy density $\boldsymbol{V_{bcp}}$. [b]: Energy density $\boldsymbol{H_{bcp}}$. [c]: Delocalization index DI. [d]: Both Ag-N bonds of Ag_2-EA_2 are equivalent. PBE-D3/def2TZVP level of calculation.

Compound	ρ_{bcp}	$\Delta\rho_{bcp}$	V_{bcp} [a]	H_{bcp} [b]	$\lvert H_{bcp}\rvert/\rho_{bcp}$	$\lvert V_{bcp}\rvert/G_{bcp}$	DI [c]	E_{int} (eV)
$Ag-EA$	0.0487	+0.161	-0.05197	-0.00583	0.12	1.13	0.50	0.707
Ag_2-EA	0.0636	+0.239	-0.07683	-0.00851	0.13	1.12	0.51	1.045
Ag_2-EA_2 [d]	0.0541	+0.196	-0.06190	-0.00646	0.12	1.12	0.45	0.842

The QTAIM descriptors of the Ag-N bonds in the three compounds are comparable (Table 3). According to the classification of Bianchi *et al.*,[40] their $\lvert \boldsymbol{V_{bcp}} \rvert/\boldsymbol{G_{bcp}}$ ratio (1.12) refers to the intermediate bond regime ($1 < \lvert \boldsymbol{V_{bcp}} \rvert/\boldsymbol{G_{bcp}} < 2$) included between ionic and covalent bonding. According to the Macchi's classification,[41] their weak electron density values ($\boldsymbol{\rho_{bcp}} \leq$ 0.06 a.u.), their large positive Laplacian values ($\Delta\boldsymbol{\rho_{bcp}} \geq 0.160$ a.u.) and small negative energy densities $\boldsymbol{H_{bcp}}$, are in favor of a dative bond of strong ionic character (Table 3). Values of DI (0.5) and $\lvert \boldsymbol{H_{bcp}} \rvert/\boldsymbol{\rho_{bcp}}$ (≈ 0.12) are also in favor of a weak covalence degree of these Ag-N bonds. The Ag-N bond strength as measured by the Espinosa's interaction energy (E_{int}) within the QTAIM electron density topological analysis,[42] decreases in the following order $Ag_2-EA > Ag_2-EA_2 > Ag-EA$ (Table 3). The same bond strength order, $Ag_2-EA > Ag-EA$, was found from the energy analysis of section 2 of this work. Both the above absolute values of coordination energies are however calculated much smaller than E_{int} values, for example E_{coord} = 0.401 *versus* E_{int}= 0.707 eV for $Ag-EA$, 0.773 *versus* 1.045 eV for Ag_2-EA (Table 1 and 3).

Espinosa's interaction energies (E_{int}) were proposed on the basis of the QTAIM analysis of experimental electron densities for a large number of X-H…O (X = C, N, O) hydrogen bonds.[42] From the comparison of the exponential correlation of the potential density energies (V_{bcp}) with the H…O distance on the one hand, and the similar exponential correlation of calculated dissociation energies of the hydrogen bonds with the H…O distance on the other hand, the $E_{int} = 0.5\ V_{bcp}$ relationship was disclosed. Note that in the present work, positive values of E_{int} were used, namely E_{int} = -0.5 V_{bcp}. The universality and the reliability of these interaction energies have been discussed in the literature.[67] They have been successfully used for investigating other weak, strong or medium strength non-covalent interactions, [67, 68] as well as

for describing interactions of weak covalence degree such as nickel-triflate[22] or metallophilic interactions [21,23] However, they might be anticipated to be less reliable for studying stronger dative bonds. It is noticeable however that a very good agreement between E_{int} values of Au-PPh_3 bonds and the corresponding calculated dissociation energies were reported. [69] Likewise, E_{int} values of Gd-OH_2 bonds comparable to sublimation enthalpies measurements,[70] were also reported. As highlighted above and in previous work,[23] E_{int} values are therefore expected to be reliable for Ag-EA bonds.

Both the bond strength and covalence degree of these Ag(0)-N bonds are much weaker than the one reported for the Ag(I)-N bonds in the silver-amidinate precursors of NPs[23] exhibiting larger QTAIM descriptors (DI = 0.63, $|\boldsymbol{H}_{\mathbf{bcp}}|/\boldsymbol{\rho}_{\mathbf{bcp}} \approx 0.21$ and E_{int} = 1.87 eV) especially E_{int} values about twice the ones of this work (0.7-1.1 eV range, Table 3). This is expected from the much weaker ionic character of the present Ag(0)-N bonds as compared to the Ag(I)-N bonds of reference 23.

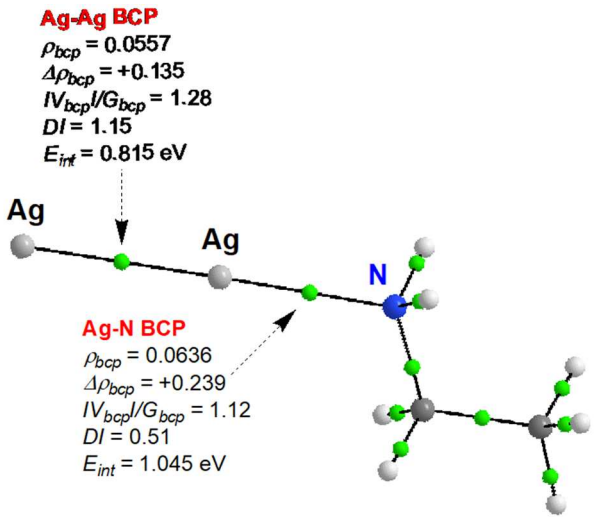

Figure 7. QTAIM molecular graph of $Ag_2 - EA$. Bond critical points (BCPs) are located as small green spheres. Nitrogen atom as a blue sphere, silver atoms in grey, carbon atoms in dark grey and hydrogen atoms in white color. See main text and Table 3 and 4 for the definition of BCP descriptors. PBE-D3/def2TZVP level of calculation.

In the three compounds of Table 4, the $|\boldsymbol{V}_{\mathbf{bcp}}|/\boldsymbol{G}_{\mathbf{bcp}}$ ratio of the Ag-Ag bond also refers to the intermediate bond regime, but is larger than the one of Ag-N bonds (1.24-1.32 range *versus* 1.12), suggesting stronger covalent degrees of Ag-Ag bonds. The QTAIM descriptors are consistent with the typical signature of metallic bonding, namely, weak electron density

values ($\boldsymbol{\rho_{bcp}} \leq 0.06$ a.u.), large positive Laplacian values ($\Delta\boldsymbol{\rho_{bcp}} \geq 0.120$ a.u.) and small negative energy densities $\boldsymbol{H_{bcp}}$. [21,71] The large DI values, consistent with a single Ag-Ag bond are slightly decreasing upon coordination of one and two EA ligands on Ag_2, while the strength of the Ag-Ag bond appears to be almost constant over the series ($E_{int} \approx 0.82$ eV).

Table 4. QTAIM descriptors (in a.u.) of the bond critical points (BCP) related to Ag-Ag bonds in Ag_2, $Ag_2 - EA$, $Ag_2 - EA_2$ compounds. BCP location is illustrated for Ag_2EA in Figure 7. [a]: Potential energy density $\boldsymbol{V_{bcp}}$. [b]: Energy density $\boldsymbol{H_{bcp}}$. [c]: delocalization index DI. PBE-D3/def2TZVP level of calculation.

Compound	ρ_{bcp}	$\Delta\rho_{bcp}$	V_{bcp} [a]	H_{bcp} [b]	$\lvert H_{bcp} \rvert / \rho_{bcp}$	$\lvert V_{bcp} \rvert / G_{bcp}$	DI [c]	E_{int} (eV)
Ag_2	0.0533	+0.148	-0.06040	-0.01170	0.22	1.24	1.30	0.822
$Ag_2 - EA$	0.0557	+0.135	-0.05993	-0.01131	0.23	1.28	1.15	0.815
$Ag_2 - EA_2$	0.0582	+0.120	-0.05890	-0.0144	0.25	1.32	1.10	0.801

The ELF topological analysis and signatures of the Ag-Ag and Ag-N bonds of Ag_2, $Ag - EA$, $Ag_2 - EA$, $Ag_2 - EA_2$ compounds, calculated at the PBE-D3/def2TZVP level, are displayed in Figure 8 and Table 5.

The Ag-N bonds are characterized by the ELF descriptors of the monosynaptic V(N) attractors. Both their large covariance with C(Ag) (0.17 or 0.20 in absolute value) and their sizeable QTAIM atomic contributions of Ag close to 3 % (Table 3), are analogous to those previously reported for the Cu-N dative bond in copper-imidazole complexes (0.17 and 5% respectively),[72] or for the dative Ag-N bond in silver-amidinate complexes (0.23 and 3% respectively)[23] exhibiting a weak covalence degree in agreement with the above QTAIM analysis (see for example $\lvert \boldsymbol{H_{bcp}} \rvert / \boldsymbol{\rho_{bcp}} \approx 0.12$, Table 3).

The QTAIM atomic charge of Ag is indicative of a very weak charge transfer (0.1 *e*) from EA to Ag in $Ag - EA$, $Ag_2 - EA$, $Ag_2 - EA_2$. It is however noticeable that this value is very close to the accuracy limit of the present QTAIM analysis. This very weak charge transfer was already mentioned above from the Bader's population analysis on VASP charge densities (Table 2). The weakening of the population of V(N) down to about 2 *e* upon coordination of EA to one silver atom or to a silver dimer (Figure 8 and Table 5), may be also related to this N to Ag charge transfer, resulting in the polarization of the silver dimer into $Ag^{\beta-} - Ag^{\psi+} - (EA)^{\delta+}$.

The ELF descriptors of the Ag-Ag bonds are consistent with a strong charge-shift bonding component, typical of the metallic bond, as evidenced by the large covariance (Cov.

column in Table 5) between both core basins C(Ag).[21] The EA coordination weakens however this charge-shift character of the Ag-Ag bond and conversely strengthens its covalence degree already mentioned in the above QTAIM analysis (see $|\boldsymbol{V}_{\mathbf{bcp}}|/\boldsymbol{G}_{\mathbf{bcp}}$ and $|\boldsymbol{H}_{\mathbf{bcp}}|/\boldsymbol{\rho}_{\mathbf{bcp}}$ in Table 4). Indeed, for $Ag_2 - EA_2$, the population of the disynaptic valence basin V(Ag, Ag) increased up to 2 *e,* from 1.36 *e* in Ag_2 and in $Ag_2 - EA$, while the electron delocalization between Ag cores, as measured by the covariance value, namely $< \bar{\sigma}^2$(C(Ag), C(Ag))> = -0.12, is much weaker than for Ag_2 (-0.27) and for $Ag_2 - EA$ (-0.23). Surprisingly, from the ELF picture, $Ag_2 - EA_2$ may not be considered as the coupling of two $Ag - EA$ fragments only (Table 5). The monosynaptic basins V(Ag) of $Ag - EA$, referring to the radical character of the fragments, exhibit a population of 0.5 *e* only and less than half of the total spin density, while the other half of the spin density is mainly located in the core basin C(Ag).

Table 5. ELF descriptors of Ag-N and Ag-Ag bonds in Ag_2, $Ag-EA$, Ag_2-EA, Ag_2-EA_2 compounds. [a]:Average population $\bar{N}$ of the monosynaptic valence basin V(N) (in *e*) [b]:QTAIM atomic contribution of Ag to V(N). [c]:covariance < $\bar{\sigma}^2$(V(N), C(Ag))>. [d]:Average population $\bar{N}$ of the disynaptic valence basin V(Ag, Ag) (in *e*). [e]:QTAIM atomic contribution of each Ag atom to V(Ag,Ag). [f]: covariance < $\bar{\sigma}^2$(C(Ag), C(Ag))>. [g]: QTAIM atomic charge (in *e)* PBE-D3/def2TZVP level of calculation.

		ELF descriptors			
Bond	Compound	V(N) [a]	%Ag [b]	Cov. [c]	q(N)[g]
Ag-N	EA	2.20	-	-	-1.1
	$Ag-EA$	2.03	0.05 (2.4%)	-0.18	-1.1
	Ag_2-EA	2.06	0.08 (3.9%)	-0.20	-1.1
	Ag_2-EA_2	2.07	0.07 (3.4%)	-0.17	-1.1
		V(Ag,Ag) [d]	%Ag [e]	Cov. [f]	q(Ag)[g]
Ag-Ag	Ag_2	1.36	0.66(49%) 0.70 (51%)	-0.27	0.0 (0.0)
	$Ag-EA$	0.52 (V(Ag))	-		-0.1
	Ag_2-EA	1.36	0.46(35%) 0.88 (65%)	-0.23	+0.1 (-0.2)
	Ag_2-EA_2	1.92	0.92(48%) 0.98 (52%)	-0.12	-0.1(-0.1)

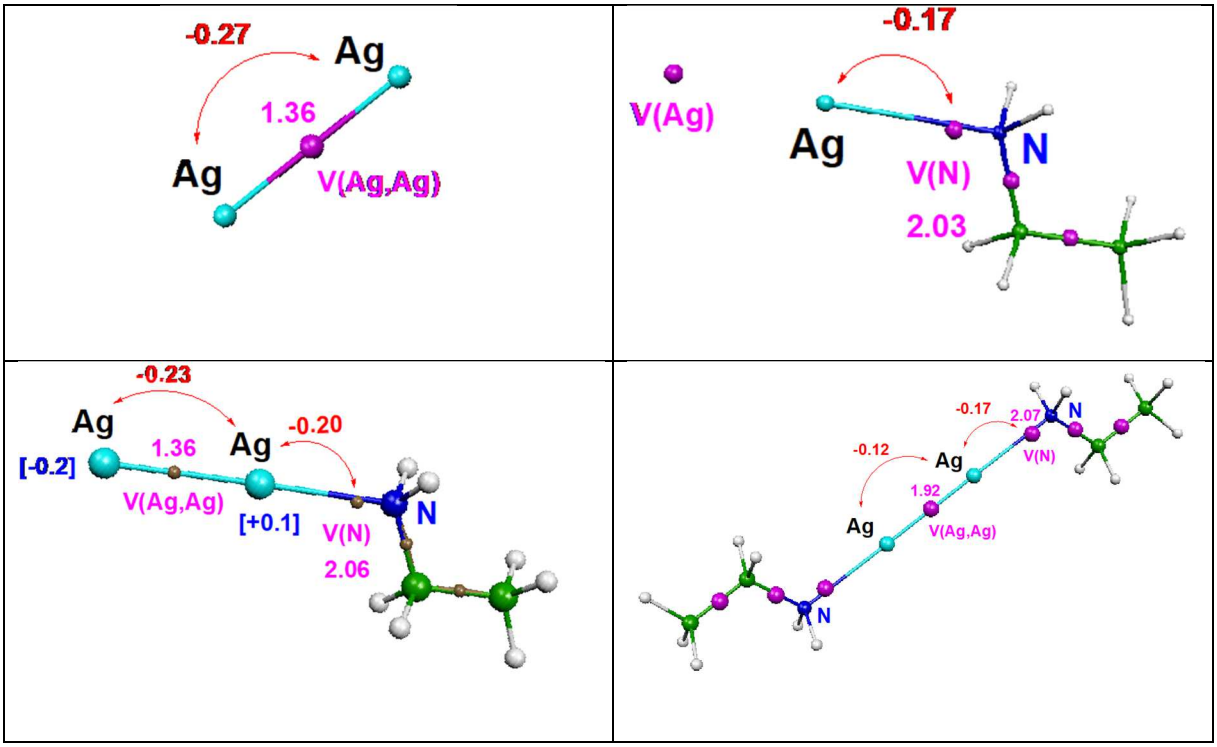

Figure 8. ELF topological analysis of Ag_2, $Ag-EA$, Ag_2-EA, Ag_2-EA_2 compounds**.** Maps of ELF attractors (small brown spheres or red stars), displaying in magenta their average populations (in *e*), covariances values in red and selected QTAIM atomic charges in blue brackets (in *e*). Nitrogen atoms in blue spheres, silver atoms in cyan, carbon atoms in green and hydrogen atoms in white color. Descriptors are averaged over equivalent bonds. PBE-D3/def2TZVP level of calculation.

Table 6. Comparison of Ag-Ag relevant ELF and QTAIM descriptors (in a.u.) calculated at the PBE-D3/def2TZVP level. [a]: ELF covariance $< \bar{\sigma}^2(C(Ag), C(Ag))>$. [b]: Ag-Ag interaction energy values in italics in eV [c]: IQA energy contributions in a.u. B3PW91/6-31G**/LANL2DZ*(Ag) level of calculation.

	Ag_2	$Ag_2 - EA$	$Ag_2 - EA_2$
Ag-Ag distance (Å)	2.561	2.560	2.567
$\lvert \boldsymbol{H}_{\mathbf{bcp}} \rvert / \boldsymbol{\rho}_{\mathbf{bcp}}$	0.22	0.23	0.25
DI	1.30	1.15	1.10
Covariance[a]	-0.27	-0.20	-0.12
E^{IQA}_{int} [c]	-0.161	-0.159	-0.159
	-4.377 [b]	*-4.317* [b]	*-4.325* [b]
V^{IQA}_{cl} [c]	7.68 10^{-3}	5.48 10^{-3}	8.98 10^{-3}
	0.209 [b]	*0.149* [b]	*0.209* [b]
V^{IQA}_{xc} [c]	-0.169	-0.164	-0.168
	-4.570 [b]	*-4.466* [b]	*-4.588* [b]

This bonding picture is tentatively refined through IQA analysis of the Ag-Ag bond in Ag_2, $Ag_2 - EA$, $Ag_2 - EA_2$ (Table 6). The major covalent contribution of the Ag-Ag bond, evidenced from large V^{IQA}_{xc} values (Table 6), is very little decreasing upon coordination of one EA ligand to Ag_2. This descriptor appears therefore less sensitive than ELF covariance or DI to measure the relative contributions of the charge-shift character and covalence degree of the Ag-Ag bond (Table 4 and 5). Similarly, from this IQA picture, the Ag-Ag bond in $Ag_2 - EA_2$ appears to be very similar to Ag_2, in contrast to the above picture based on other ELF and QTAIM descriptors.

E^{IQA}_{int} values appear to be much lower than Espinosa's E_{int} interaction energies, suggesting different meanings as already discussed.[23]

However, they appear to strongly underestimate the Ag-Ag bond strength as compared to E_{bind} and E^{IQA}_{int} values (Table 6). This suggest that E_{int} values are not reliable for describing strong metallic Ag-Ag bonds.

Furthermore, E_{int} values are restricted for the discussion of bond strength while Energy Decomposition Analysis (EDA) schemes allow for the analysis of the various stabilizing or

destabilizing energetic components of the bond. IQA was selected as pointed out by Paul Popelier,[73] the results may be related to known chemical concept "*IQA is an Energy Decomposition Analysis scheme, defining the following chemical concepts: covalency (via exchange), ionicity and polarity (via electrostatics), dispersion via electron correlation and steric effects (via the intra-atomic or self-energy*)".

CONCLUSIONS

To study the influence of an amine ligand on the structure and stability of Ag very first nuclei, DFT computational studies have been performed in order to characterize the structure, the atomic charge distribution and the 2D/ 3D relative stability of small-size silver clusters Ag_n ($2 \leq n \leq 7$) coordinated or not to one ethylamine ligand. Moreover, the effect on the 2D/3D silver clusters transition of EA saturation ($Ag_n - EA_n$) is investigated. Finally, topological analyses (ELF and QTAIM) have been performed to finely characterise the nature and strength of the Ag-Ag and Ag-N bonds.

The most stable geometries of the bare 2D and 3D clusters and the associated 2D/3D transition range were found in good agreement with the literature. Moreover, the coordination energies of one EA molecule on silver clusters were similar to the ones reported for ammonia adsorption on such Ag_n clusters. Our results evidenced that the EA coordination induces a shift of the transition from 2D to 3D structures from n = 7 to n = 6. This shift has been explained by a much stronger EA binding on the Ag_5^{3D} and Ag_6^{3D} over the 2D ones, which counterbalances the bare Ag_n clusters relative stabilities. QTAIM analysis on charge densities showed that the EA coordination also leads to an increase in the silver clusters polarization thanks to an electron transfer from the ligand to the metal. For fully EA saturated silver clusters $Ag_n - EA_n$, the effect on the 2D/3D transition is even more pronounced with a shift to n = 5.

ELF and QTAIM topological analyses were performed on selected systems to finely characterize Ag-N and Ag-Ag bonding upon coordination of one or two EA ligands to one silver atom or to the silver dimer. The Ag-N bonds were characterized as dative bonds of strong ionic character and the Ag-Ag ones as charge-shift metallic bonds. The EA coordination weakens the charge-shift character of the Ag-Ag bond and conversely strengthens its covalence degree which is maximum in $Ag_2 - EA_2$. The ELF and QTAIM analyses have confirmed the electron transfer from EA to the coordinated silver atom and its first neighbours, inducing the polarisation of the metallic core and resulting in an $Ag^{\beta-} - Ag^{\gamma+} - (EA)^{\delta+}$ picture.

The strength of the charge-shift metallic Ag-Ag bonds and their covalence degree have been characterized using ELF and QTAIM descriptors and IQA analysis.

These topological analyses will be extended to larger-size silver clusters Ag_n (n > 2). In addition, this work will be followed by the study of the coordination of amines ligands on silver nanoparticles and extended surfaces and of the competitive adsorption between the amidine molecules released by the precursors and the amine used as NP stabilisers.

Supporting Information: Additional structural and energy data of Ag_n , $Ag_n - EA$ ($2 \leq n \leq 7$) and $Ag_n - EA_n$ ($4 \leq n \leq 6$) clusters.

Acknowledgements

The theoretical studies were performed using HPC resources from CALMIP (Grants 2018-2020 [16028]]) and from GENCI-[CINES/IDRIS] (Grants 2018-2020 [0805008]). The authors wish to acknowledge the financial support of the Centre National de la Recherche Scientifique (CNRS).

References

[1] Natsuki, J.; Natsuki, T.; Hashimoto, Y. A Review of Silver Nanoparticles: Synthesis Methods, Properties and Applications, *Int. J. Mater. Sci. Appl.* **2015**, *4*, 325-332.

[2] Zhang, X. F.; Liu, Z. G.; Shen, W.; Gurunathan, S. Silver Nanoparticles: Synthesis, Characterization, Properties, Applications, and Therapeutic Approaches. *Int. J. Mol. Sci*. 2016, *17*, 1534-1568.

[3] Sun, Y. Controlled Synthesis of Colloidal Silver Nanoparticles in Organic Solutions: Empirical Rules for Nucleation Engineering. *Chem. Soc. Rev.* **2013**, *42*, 2497−2511.

[4] Battocchio, C.; Meneghini, C.; Fratoddi, I.; Venditti, I.; Russo, M. V.; Aquilanti, G.; Maurizio, C.; Bondino, F.; Matassa, R.; Rossi, M.; Mobilio, S.; Polzonetti, G. Silver Nanoparticles Stabilized with Thiols: A Close Look at the Local Chemistry and Chemical Structure *J. Phys. Chem. C* **2012**, *11*6, 19571-19578.

[5] Cure, J.; Coppel, Y.; Dammak, T.; Fazzini, P. F.; Mlayah, A.; Chaudret, B.; Fau, P. Monitoring the Coordination of Amine Ligands on Silver Nanoparticles Using NMR and SERS *Langmuir*, **2015**, *31*, 1362-1367.

[6] Shao, X.; Liu, X.; Cai, W. Structural Optimization of Silver Clusters up to 80 Atoms with Gupta and Sutton−Chen Potentials. *J. Chem. Theory Comput.* **2005**, *1*, 762−768.

[7] Oliveira, L.; Tarrat, N.; Cuny, J; Morillo, J.; Lemoine, D.; Spiegelman F.; Rapacioli, M. Benchmarking DFTB for silver and gold materials: from small clusters to bulk *J. Phys. Chem. A* **2016**, *120*, 8469-8483.

[8] Cuny, J; Tarrat, N.; Spiegelman F.; Huguenot, A; Rapacioli, M Density-functional tight-binding approach for metal clusters, nanoparticles, surfaces and bulk: application to silver and gold. *J. Phys.: Condens. Matter* **2018**, *30*, 303001/1-21

[9] Loffreda, D.; Foster, D. M.; Palmer, R. E.; Tarrat, N. Importance of defective and nonsymmetric structures in silver nanoparticles *J. Phys. Chem. Lett.* **2021**, *12*, 3705−3711.

[10] Yu, C; Schira, R.; Brune, H.; von Issendorff, B.; Rabilloud, F.; Harbich, W. Optical properties of size selected neutral Ag clusters: electronic shell structures and the surface plasmon resonance *Nanoscale* **2018**, *10*, 20821-20827.

[11] Chen, M.; Dyer, J.E.; Li, K.; Dixon, D.A. Prediction of structures and atomization energies of small silver clusters, (Ag)n, n>100 *J. Phys. Chem. A* **2013**, *117*, 8298-8313.

[12] Cardini, G.; Muniz-Miranda, M.; Pagliai, M.; Schettino, V. A density functional study of the SERS spectra of pyridine adsorbed on silver clusters. *Theor Chem Acc* **2007**, *117*, 451–458.

[13] Martínez, A. Bonding interactions of metal clusters [Mn (M= Cu, Ag, Au; n=1-4)] with ammonia. Are the metal clusters adequate as a model of surfaces? *J. Brazil. Chem. Soc*. **2005**, *16*, 337-344.

[14] Srinivas S.; Salian U.A.; Jellinek J. Theoretical Investigations of Silver Clusters and Silver-Ligand Systems. In: Russo N., Salahub D.R. (eds) Metal-Ligand Interactions in Chemistry, Physics and Biology. Springer, Dordrecht. NATO Science Series (Series C: Mathematical and Physical Sciences), **2000**, *546*, 295-324.

[15] Coulson, C. A. Valence. Oxford, Clarendon Press, 1952.

[16] (a) Kitaura, K.; Morokuma, K. A new energy decomposition scheme for molecular interactions within the Hartree-Fock approximation. *Int. J. Quant. Chem.* **1976**, *10*, 325-340. (b) Ziegler, T.; Rauk, A. On the calculation of bonding energies by the Hartree Fock Slater method. *Theor. Chim. Acta* **1977**,*46*,1−10.

[17] Pauling, L. The Nature of the Chemical Bond; Cornell University Press, Ithaca, NY, **1939** (3rd ed., **1960**).

[18] (a) Becke, A. D.; Edgecombe, K. E. A simple measure of electron localization in atomic and molecular systems *J. Chem. Phys.* **1990**, *92*, 5379-5403. (b) Silvi, B.; Savin, A. Classification of chemical bonds based on topological analysis of electron localization function. *Nature*, **1994**,

371, 683-686.

[19] Silvi, B.; Fourré, I.; Alikhani, M. E. The Topological Analysis of the Electron Localization Function. A Key for a Position Space Representation of Chemical Bonds. *Monatshefte für Chemie* **2005**, *136*, 855-879.

[20] Bader, R. F. W.; Atoms In Molecules: A Quantum Theory, Clarendon Press, Oxford, UK, 1990.

[21]Lepetit, C.; Fau, P.; Fajerwerg, K.; Kahn, M. L.; Silvi, B. Topological analysis of the metal-metal bond: a tutorial review. *Coord. Chem. Rev.* **2017**, *345*, 150-181.

[22]Lepetit, C.; Vabre, B.; Canac,Y.; Alikhani, M. E.; Zargarian D. Pentacoordinated, Square-Pyramidal Cationic PCPNi(II) Pincer Complexes: ELF and QTAIM TopologicalAnalyses of Nickel-Triflate Interactions. *Theor. Chem. Acc.* **2018**, 137:141.

[23] Puyo, M.; Lebon, E.; Vendier, L.; Kahn, M. L.; Fau, P.; Fajerwerg, K.; Lepetit, C. Topological Analysis of Ag–Ag and Ag–N Interactions in Silver Amidinate Precursor Complexes of Silver Nanoparticles *Inorg. Chem.* **2020**, *59*, 4328-4339.

[24] Kresse, G.; Furthmüller, Efficiency of ab-initio total energy calculations for metals and semiconductors using a plane-wave basis set *J. Comput. Mat. Sci.* **1996**, *6*, 15-50.

[25] Kresse, G.; Furthmüller, Efficient iterative schemes for ab initio total-energy calculations using a plane-wave basis set *J. Phys. Rev. B* **1996**, *54*, 11169-11186.

[26] Kresse, G.; Hafner, Ab initio molecular dynamics for liquid metals J. *Phys. Rev. B* **1993**, *47*, 558-561.

[27] Blöchl, P. E., Projector augmented-wave method *Phys. Rev. B* **1994**, *50*, 17953-17979.

[28] Kresse, G.; Joubert, D., From ultrasoft pseudopotentials to the projector augmented-wave method *Phys. Rev. B* **1999**, *59*, 1758-1775.

[29] Banerjee, J.; Behnle, S.; Galbraith, M. C. E.; Settels, V.; Engels, B.; Tonner, R.; Fink, R. F. Comparison of the Periodic Slab Approach with the Finite Cluster Description of Metal–Organic Interfaces at the Example of PTCDA on Ag(110). *J. Comput. Chem*. **2018**, *39*, 844-852.

[30] Contreras-Torres, F. F. Dispersion-Corrected Density Functional Theory Study of the Noncovalent Complexes Formed with Imidazo[1,2-a]pyrazines Adsorbed onto Silver Clusters *ACS Omega* **2020**, *5*, 561-569.

[31] Fernandez, E. M.; Balbas, L. C. Study of odd–even effects in physisorption and chemisorption of Ar, N_2, O_2 and NO on open shell Ag_{11-13}+clusters by means of self-consistent van der Waals density functional calculation *Phys. Chem. Chem. Phys.* **2019**, *21*, 25158-25174.

[32] Dion, M.; Rydberg, H.; Schröder, E.; Langreth, D. C.; Lundqvist, B. I. Van der Waals Density Functional for General Geometries. *Phys. Rev. Lett.* **2004**, *92*, 246401/1-4.

[33] Methfessel, M.; Paxton, A. T., High-precision sampling for Brillouin-zone integration in metals *Phys. Rev. B* **1989**, 40, 3616-3621.

[34] https://www.ccdc.cam.ac.uk/.../ccdcresources/Elemental_Radii.xlsx

[35]Henkelman, G.; Arnaldsson, A.; Jónsson, H. A fast and robust algorithm for Bader decomposition of charge density. *Comput. Mat. Sci.* **2006**, *36*, 354-360.

[36]Sanville, E.; Kenny, S. D.; Smith, R.; Henkelman, G. An improved grid-based algorithm for Bader charge allocation *J. Comput. Chem.* **2007**, *28*, 899-908.

[37]Tang, W.: Sanville, E.; Henkelman, G. A grid-based Bader analysis algorithm without lattice bias. *J. Phys. Condens. Matter* **2009**, *21*, 084204/1-7.

[38]Yu, M.; Trinkle, D. R. Accurate and efficient algorithm for Bader charge integration. *J. Chem. Phys.* **2011**, *134*, 064111.

[39] Frisch, M. J.; Trucks, G. W.; Schlegel, H. B.; Scuseria, G. E.; Robb, M. A.; Cheeseman, J. R.; Scalmani, G.; Barone, V.; Mennucci, B.; Petersson, G. A.; Nakatsuji, H.; Caricato, M.; Li, X.; Hratchian, H. P.; Izmaylov, A. F.; Bloino, J.; Zheng, G.; Sonnenberg, J. L.; Hada, M.; Ehara, M.; Toyota, K.; Fukuda, R.; Hasegawa, J.; Ishida, M.; Nakajima, T.; Honda, Y.; Kitao, O.; Nakai, H.; Vreven, T.; Montgomery, J. A., Jr.; Peralta, J. E.; Ogliaro, F.; Bearpark, M.; Heyd, J. J.; Brothers, E.; Kudin, K. N.; Staroverov, V. N.; Kobayashi, R.; Normand, J.; Raghavachari, K.; Rendell, A.; Burant, J. C.; Iyengar, S. S.; Tomasi, J.; Cossi, M.; Rega, N.; Millam, J. M.; Klene, M.; Knox, J. E.; Cross, J. B.; Bakken, V.; Adamo, C.; Jaramillo, J.; Gomperts, R.; Stratmann, R. E.; Yazyev, O.; Austin, A. J.; Cammi, R.; Pomelli, C.; Ochterski, J. W.; Martin, R. L.; Morokuma, K.; Zakrzewski, V. G.; Voth, G. A.; Salvador, P.; Dannenberg, J. J.; Dapprich, S.; Daniels, A. D.; Farkas, Ö.; Foresman, J. B.; Ortiz, J. V.; Cioslowski, J.; Fox, D. J. Gaussian 09, Revision D.01; Gaussian, Inc.: Wallingford, CT, 2009.

[40] (a) Bianchi, R.; Gervasio, G.; Marabello, D., Experimental Electron Density Analysis of $Mn_2(CO)10$: Metal-Metal and Metal-Ligand Bond Characterization. *Inorg. Chem.* **2000,** *39* (11), 2360-2366. (b) E. Espinosa, I. Alkorta, J. Elguero, E. Molins J. Chem. Phys. **117**, 5529-5542 (2002)

[41] Macchi, P.; Proserpio, D. M.; Sironi, A., Experimental Electron Density in a Transition Metal Dimer: Metal-Metal and Metal-Ligand Bonds. *J. Am. Chem. Soc.* **1998,** *120* (51), 13429-13435.

[42] (a) E. Espinosa, E. Molins, C. Lecomte Hydrogen bond strengths revealed by topological analyses of experimentally observed electron densities Chem. Phys. Lett. **285**, 170-173 (1998) (b) E. Espinosa, I. Alkorta, I. Rozas, J. Elguero, E. Molins About the evaluation of the local

kinetic, potential and total energy densities in closed-shell interactions Chem. Phys. Lett. **336**, 457-461(2001). E_{int} = - ½ V_{bcp} and E_{int} (eV) = -13.606 x V_{bcp} (au).

[43] (a) Blanco, M. A.; Martin Pendas, A.; Franscisco E. Interacting Quantum Atoms: A Correlated Energy Decomposition Scheme Based on the Quantum Theory of Atoms in Molecules *J. Chem. Theory Comput.* **2005**, *1*,1096-1109. (b); Franscisco E.; Martin Pendas, A.; Blanco, M. A. A Molecular Energy Decomposition Scheme for Atoms in Molecules *J. Chem. Theory Comput.* **2006**, *2*, 90-102. (c) Maxwell, P.; Martin Pendas, A.; Popelier, P. L. A. Extension of the interacting quantum atoms (IQA) approach to B3LYP level density functional theory (DFT). *Phys. Chem. Chem. Phys.* **2016**, *18*, 29086-21000.

[44] Tognetti,V.; Joubert, L. On Atoms-in-Molecules Energies from Kohn–Sham Calculations. *ChemPhysChem* 2017, *18*, 2675–2687. Suarez, D.; Dıaz, N.; Francisco, E.; Martın Pendas, A. Application of the Interacting Quantum Atoms Approach to the S66 and Ionic-Hydrogen-Bond Datasets for Noncovalent Interactions *ChemPhysChem* **2018**, *19*, 973–987.

[45] (a) Cornaton, Y.; Djukic, J.-P. A noncovalent interaction insight onto the concerted metallation deprotonation mechanism. *Phys. Chem. Chem. Phys.* **2019**, *21*, 20486-20498. (b) Pastorczak, E.; Corminboeuf, C. Perspective: Found in translation: Quantum chemical tools for grasping non-covalent interactions. *J. Chem. Phys.* **2017**, *146*, 120901/1-12.

[46] Keith T. A, AIMAll (Version 17.11.14), TK Gristmill Software, Overland Park KS, USA, **2016** (aim.tkgristmill.com).

[47] Poater. J.; Duran, M.; Sola, M.; Silvi, B. Theoretical Evaluation of Electron Delocalization in Aromatic Molecules by Means of Atoms in Molecules (AIM) and Electron Localization Function (ELF) Topological Approaches. *Chem. Rev.* **2005**, *105*, 3911-3947.

[48] Silvi, B.; Gillespie, R. J.; Gatti, C. Electron density analysis. in *Comprehensive Inorganic Chemistry II* **2013**, *9*, 187-226.

[49] Silvi, B. How topological partitions of the electron distributions reveal delocalization. *Phys. Chem. Chem. Phys.* **2004,** *6*, 256-260.

[50] Lepetit, C.; Silvi, B.; Chauvin, R. ELF Analysis of Out-of-Plane Aromaticity and In-Plane Homoaromaticity in Carbo[*N*]annulenes and [*N*]Pericyclynes. *J. Phys. Chem. A* **2003**, *107*, 464-473**.**

[51] Noury, S.; Krokidis, X.; Fuster, F.; Silvi, B. Computational tools for the electron localization function topological analysis. *Comput. & Chem.***1999**, *23*, 597-604.

[52]Kahnouji, H.; Najafvandzadeh, H.; Hashemifar, S. J.; Alaei, M.; Ak- Barzadeh, H. Density-functional study of the pure and palladium doped small copper and silver clusters *Chem. Phys. Lett.* **2015**, *630*, 101-105.

[53] Wang, C.; Yang, Y.; Liu, X.; Li, Y.; Song, D.; Tian, Y.; Zhang, Z.; Shen X. Dissociative chemisorption of O_2 on Ag_n and $Ag_{n-1}Ir$ (n = 3–26) clusters: a first-principle study *Phys. Chem. Chem. Phys.* **2020**, *22*, 9053-9066.

[54] Gamboa, G.U.; Reber, A. C.; Khanna, S. N. Electronic subshell splitting controls the atomic structure of charged and neutral silver clusters *New J. Chem.* **2013**, *37*, 3928-3935.

[55] Fournier, R. Theoretical study of the structure of silver clusters *J. Chem. Phys.* **2001**, *115*, 2165-2177.

[56]Idrobo, J. C.; Ogut, S.; Jellinek, J. Size dependence of the static polarizabilities and absorption spectra of Agn(n=2–8) clusters *Phys. Rev. B* **2005**, *72*, 085445-085453.

[57]Singh, A.; Majumder, C.; Sen, P. Do Agn (up to n = 8) clusters retain their identity on graphite? Insights from first principles calculations including dispersion interactions *J. Chem. Phys.* **2014**, *140*, 164705-164712.

[58] Oliveira, L. F. L.; Tarrat, N.; Cuny, J.; Morillo, J.; Lemoine, D.; Spiegelman, F.; Rapacioli M. Benchmarking Density Functional Based Tight-Binding for Silver and Gold Materials: From Small Clusters to Bulk *J. Phys. Chem. A* **2016**, *120*, 8468-8483.

[59] McKee, M.L.; Samokhvalov, A. Density Functional Study of Neutral and Charged Silver Clusters Agn with n = 2–22. Evolution of Properties and Structure *J. Phys. Chem. A* **2017**, *121*, 5018-5028.

[60] Kittel, C., In Introduction to solid state physics; Fifth edition; Wiley: United Kingdom, 1976.

[61] Rayner, D. M.; Athanassenas, K.; Collings, B. A.; Mitchell A. S.; Hackett, P. A. Silver Clusters and Silver Cluster/Ammonia Complexes; In: Jellinek J. (eds) Theory of Atomic and Molecular Clusters. Springer Series in Cluster Physics. Springer, Berlin, Heidelberg, pp 371-395.

[62] Gulbransen, J. L.; Fitchett, C. M. Anion directed control of supramolecular structure in silver complexes through weak interactions *Cryst. Eng. Comm.* **2012**, *14*, 5394-5397.

[63] Pettinari, C.; Marchetti, F.; Orbisaglia, S.; Pettinari, R.; Ngoune, J.; Gomez , M.; Santos, C.; Alvarez, E., Group 11 complexes with the bidentate di(1H-indazol-1-yl)methane and di(2H-indazol-2-yl)methane) ligands *Cryst. Eng. Comm.* **2013**, *15*, 3892-3907.

[64]Sun, Q.; Bai, Y.; He, G.; Duan, C.; Lin, Z.; Meng, Q. *Chem. Commun.* **2006**, *26*, 2777-2779.

[65] Montoya, A.; Schlunke, A.; Haynes, B. S. *J. Phys. Chem. B* **2006**, *110*, 17145-17154.

[66] Linstrom P. J.; Mallard, W.G. Eds. NIST Chemistry WebBook, NIST Standard Reference Database Number 69, National Institute of Standards and Technology, Gaithersburg MD, 20899, https://doi.org/10.18434/T4D303, (accessed December 13, 2019).

[67] (a) Spackman, M. A. How reliable are intermolecular interaction energies estimated from

topological analysis of experimental electron densities. *Cryst. Growth Des.* **2015**, 15, 5624−5628. (b) Nelyubina, Y.V.; Antipin, M.Y.; Lyssenko, K. A. *Russ. Chem. Re*v. **2010**, *79*,167-187. (c) Gatti, C. Chemical bonding in crystals: new directions. *Z. Kristallogr. Cryst.* **2005**, *22*0, 399-457.

[68] Valyaev, D.A.; Brousses, R.; Lugan, N.; Fernàndez, I.; Sierra, M. A. Do ν(CO) stretching frequencies in metal carbonyl complexes unequivocally correlate with the intrinsic electron-donicity of ancillary ligands. *Chem Eur J.* **2011**, *17*, 6602-6605.

[69] Borissova, A.O.; Korlyukov, A. A., Antipin, M.Y.; Lyssenko, K. A. Estimation of dissociation energy in donor-acceptor complex AuCl•PPh3 via topological analysis of the experimental electron density distribution function. *J. Phys. Chem.* A **2008**, *112*, 11519–11522.

[70] Puntus, L. N.; Lyssenko, K. A.; Antipin, M. Y.; Bünzli, J.-C. G. Role of inner -and outer sphere bonding in the sensitization of Eu^{III}-luminescence deciphered by combined analysis of experimental electron density distribution function, and photophysical data. *Inorg. Chem.* **200**8, *47*, 1105-11107.

[71] Bianchi, R.; Gervasio, G.; Marabello, D. The experimental charge density in transition metal compounds *C. R. Chim.* **2005,** *8*, 1392-1399.

[72] Boukallaba, M.; Kerkeni, B.; Lepetit, C.; Berthomieu, D. Coordination complexes of 4-Methylimidazole with Zn^{II} and Cu^{II} in gas phase and in water: A DFT Study. *J. Mol. Model.* **2016**, *22*, 301/1-10.

[73] Andrés, J.; Ayers, P. W.; Boto, R. A.; Carbó-Dorca, R.; Chermette, H.; Cioslowski, J.; Contreras-García, J.; Cooper, D. L.; Frenking, G.; Gatti, C.; Heidar-Zadek, F.; Joubert, L.; Pendás, A. M.; Matito, E.; Mayer, I.; Misquitta, A. J.; Mo, Y.; Pilmé, J.; Popelier, P. L. A.; Rahm, M.; Ramos-Cordoba, E.; Salvador, P.; Schwarz, W. H. E.; Shahbazian, S.; Silvi, B.; Solà, M.; Szalewicz, K.; Tognetti, V.; Weinhold, F.; Zins E.-L. Nine questions on energy decomposition analysis. *J. Comput. Chem*. **2019**, *40*, 2248-2283.

For Table of Contents Only

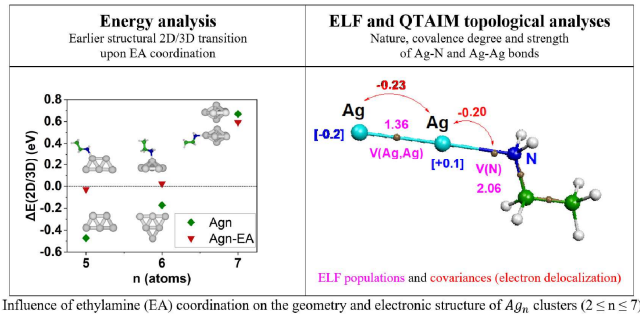

Influence of ethylamine (EA) coordination on the geometry and electronic structure of Ag_n clusters ($2 \leq n \leq 7$)

Synopsis :

The transition from 2D to 3D structures for Ag_n clusters is shifted from n = 7 for the bare clusters to n = 6 in the presence of one ethylamine (EA) coordinating ligand. The effect is even more pronounced for fully EA saturated $Ag_n - EA_n$ clusters with a shift at n = 5. ELF and QTAIM topological analyses evidence the coordinative and metallic character of the Ag-N and Ag-Ag bonds respectively.